Title
DEGRADATION OF SODIUM B - ALUMINA: EFFECT OF MICROSTRUCTURE

Authors
Buechele, A.C.
Jonghe, L.C. De

Publication Date
1981-08-01

LBL-13188
Preprint

Lawrence Berkeley Laboratory
UNIVERSITY OF CALIFORNIA

Materials & Molecular Research Division

Submitted to the Journal of the Electrochemical Society

DEGRADATION OF SODIUM β" - ALUMINA: EFFECT OF MICROSTRUCTURE

Andrew C. Buechele and Lutgard C. De Jonghe

August 1981

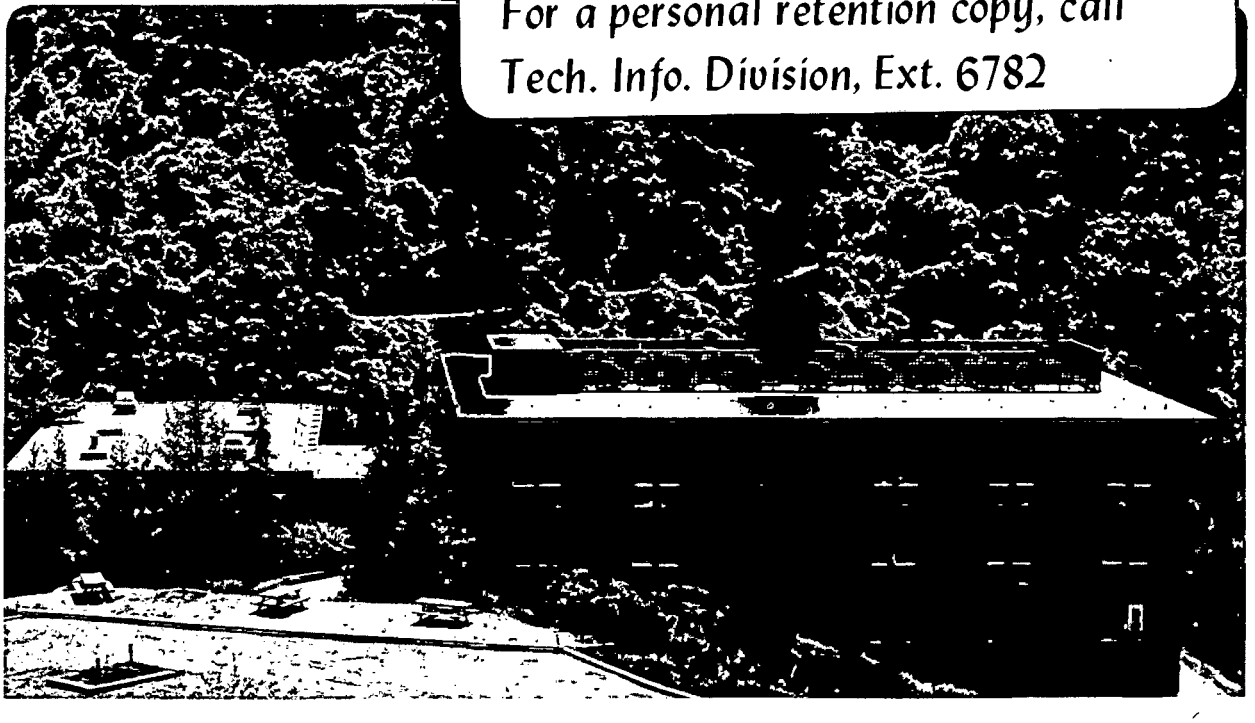

Prepared for the U.S. Department of Energy under Contract W-7405-ENG-48

DISCLAIMER

LBL-13188

DEGRADATION OF SODIUM β" - ALUMINA: EFFECT OF MICROSTRUCTURE

Andrew C. Buechele and Lutgard C. De Jonghe
Materials and Molecular Research Division
Lawrence Berkeley Laboratory

and

Department of Materials Science and Mineral Engineering
University of California, Berkeley, California 94720

---

*This work was supported by the Assistant Secretary for Conservation and Renewables, Office of Advanced Conservation Technology, Electrochemical Systems Research Division of the U. S. Department of Energy under Contract No. W-7405-ENG-48. The major funding was provided by the Electric Power Research Institute.

ABSTRACT

The effects of microstructure on failure initiation of sodium-beta" alumina solid electrolytes has been investigated by acoustic emission detection. Mode I failure initiation follows Weibull statistics with a modulus of about 2.5. The average critical current densities were 145 mA cm^{-2} and 640 mA cm^{-2} for large and for small grained electrolytes, respectively. Considerations of failure statistics indicate conditions where proof testing may be necessary to achieve sufficient reliability. These considerations assume complete equivalence between mechanical and electrolytic failure; the indication are, however, that such equivalence is not valid.

1. Introduction

When sodium-beta or beta" alumina solid electrolytes are subjected to ionic charge transfer in sodium/sodium or in sodium/sulfur cells, degradation of the electrolytes may occur. This electrochemical degradation may take different forms, as was recently discussed by De Jonghe et al. [1]. Mode I degradation involves the cathodic plating of Na into a pre-existing surface flaw on the sodium side of the electrolyte, causing crack extension above some critical value of the current density. This was first discussed by Armstrong et al. [2] (ADT). Several workers have considered refinements of the ADT treatmemt, attempting to derive theoretically the critical current density thresholds at which the Mode I crack propagation initiates or propagates [3-6]. All calculations, however, lead to predicted current density thresholds that are orders of magnitude higher than the observed ones [6]. To fully understand the factors that determine the onset of Mode I degradation it is first necessary to measure the critical current density thresholds with some accuracy and to determine which factors affect this threshold. Several experiments were done by Armstrong et al. [2] indicating that imperfections in the surface of the electrolyte indeed played a role. Further experiments on initiation of Mode I degradation were performed by Richmann and Tennenhouse [4] and by Virkar et al. [3,5]. These experiments involved strength measurements after electrolysis. A more sensitive method for the detection of initiation of crack propagation is acoustic emissions detection. Acoustic emission detection during current flow through solid electrolytes

was first reported by Worrell and Redfern [7]. The technique was adopted in the present work. Na/Na cells, using Na-beta" solid electrolytes were tested at 350°C, and the acoustic activity was monitored. Two types of electrolytes, with the same composition but different microstructures, were examined. Additionally, some electrolytes used in extended Na/S cell testing were also examined for evidence of correlation between microstructure and Mode I degradation. The results indicate that large grained electrolyte has a significantly lower current density threshold for Mode I initiation.

2. Materials

The Na/Na cell tests were performed on Na-beta" alumina tubes prepared by Ceramatec, Inc.* The electrolyte composition was: 8.85 wt Na_2O; 0.75 wt Li; balance Al_2O_3. The tubes had a wall thickness of 1.5 mm and a diameter of 19 mm. The microstructural data are summarized in Table I and the microstructures are shown in Fig. 1. The microstructure of the coarse grained material, "300", is strongly bi-modal. The fine grained material, "10", was also bi-modal, but the volume fraction of grains with a size larger than 10 μm was less than 0.01, as indicated in Table I. The grain sizes reported here were determined by a random intercept method, in which the number of grain boundaries are counted intercepting a random straight line on a micrograph. The largest grain dimensions were measured directly on individual grains.

---

*Ceramatec, Inc., 580 Arapeen Drive, Salt Lake City, Utah 84108.

Some used electrolytes were also obtained from British Rail.* The electrolyte reported on here had a nominal composition of 8.12 wt% Na_2O; 0.7 wt% Li; balance Al_2O_3. The electrolyte had been subjected to 195 cycles in a Na/S cell, over a period of 97 days, for a total (charge + discharge) charge transfer of 121 A hrs/cm^{-2} at 350°C, between 50 and 100 mA cm^{-2}.

3. Experimental

When electrolytes fail by initiation and propagation of cracks, stress waves are generated as a result of the sudden stored energy release. These stress waves, or acoustic emissions, can be monitored by a sensitive ultrasonic transducer, and either the cumulative events on the number of acoustic events per second can be recorded. In the present work the increase in count rate appeared to be the clearest indication of the onset of acoustic activity. A similar method was used by Worrell and Redfern [7].

An acoustic emission detection system manufactured by Acoustic Emission Technology Corporation+ was used. An acoustic transducer was coupled to the specimen via an alumina waveguide rod. The signals were amplified to 106 dB by the instrument amplifier, Model 204A, operating in a bandwidth between 100 and 250 kHz. It was important to ensure excellent contact at the various mechanical interfaces in the system, and to eliminate electrical and mechanical interference.

---

*British Rail, Research and Development Division, Derby, England.
+Acoustic Emission Technology Corporation, 1812J Tribute Road, Sacramento, California 95815.

The sodium/sodium cells were constructed from rings cut from the Na-beta" alumina tubes. The rings were cut under kerosene to a height of approximately 15 mm and sealed to a small disk and to a tube of α-alumina with a sealing glass.* The setup is shown in Fig. 2. Prior to welding, the electrolyte rings were carefully washed in dry ethanol and acetone and heated in air for 30 min. to about 700°C to remove all organic matter and water. In the welding operation the external surfaces of the rings were covered with sealing glass, except for a small area of about 0.2 cm^2 left exposed for current flow. The Na/Na cells were set up in an argon glove box. The sodium was obtained from Fisher Scientific Company.+ Although the oxygen contamination of glove box was below 5 ppm, it was sufficient to saturate the sodium with oxygen since Na_2O was observed to form on the surfaces of molten sodium. Oxygen saturation of the sodium is unavoidable in glove box experiments, as the Na/Na_2O equilibrium oxygen pressure is about 10^{-55} atm at 300°C.

To verify the sensitivity of the acoustic emission detection system, some electrolytes were cooled through the freezing point of sodium under a current of about 40 mA cm^{-2}, and the acoustic emission rates were compared to those of samples cooled without current passage.

---

*Package sealant IN-3, Owens-Illinois, Electronic Materials Center, Box 1035, Toledo, Ohio 43666

+Certified ACS Sodium, Fisher Scientific Company, Fair Lawn, New Jersey 07410

The possibility of large grains acting as initiation sites for Mode I degradation was examined on electrolytes with the "300" microstructure with a polished surface section. These cells were then subjected to increasing currents until failure with the polished section acting either as a sodium exit or a sodium entrance surface only. After this cycle, the cells were removed from the Na, washed in methanol, stained with $AgNO_3$ [8], and examined in the optical microscope.

4. Results and Discussions

4.1 Verification of the acoustic emission detection method

At low current densities, below 50 mA/cm^2, Mode I degradation is unlikely above the melting point of sodium. However, as the sodium becomes solid, Mode I degradation should be expected to occur. The onset of Mode I degradation should therefore be manifested as an increased acoustic emission rate at the freezing point of sodium when the current is maintained. Figure 3 shows the increase of the acoustic activity in the immediate vicinity of the freezing point of sodium. Specimens cooled through the freezing point of sodium in the same set-up without current did not exhibit any increased acoustic activity. Some additional tests at room temperature were done on barshaped samples of the electrolyte with a negative electrode of evaporated gold and a positive electrode of Hg-Na amalgam. The electrolyte next to the negative electrode could then be observed during the test. Increasing currents were passed through the sample until a sudden increase in acoustic activity occurred. Moments later, after a current increase of about 5 to 10%, the usual rapid darkening, indi-

cative of the appearance of a sodium filled crack, could be seen emanating from the negative electrode. These experiments demonstrated that acoustic emission monitoring was suitable for the study of the initiation of Mode I breakdown.

4.2 Microstructure dependence of Mode I initiation

The critical current density for initial crack propagation will be related to the largest pre-existing active flaw in the surface of the electrolyte in contact with the negative sodium electrode. The statistical nature of the active flaw distribution should then lead to a corresponding distribution of the current densities necessary to initiate Mode I degradation. Since the distribution is one of extreme values, the critical current distribution may be described using Weibull statistics. The critical current density distribution is then analogous to the distribution of mechanical strengths for a brittle solid of volume V. The standard treatment [9] gives the survival probability, P_s, as

$$P_s = 1 - P_f = \exp\{ - (V/V_o) [(\sigma - \sigma_u)/\sigma_o]^m \} \quad (1)$$

where P_f is the failure probability, σ is the applied stress, and σ_u, and m are materials constants. V_o and σ_o are normalizing parameters. By analogy, the distribution of critical current densities might be represented as

$$P_s = \exp\{ - (A/A_o) [(j - j_u)/j_o]^n \} \quad (2)$$

where A is the active electrode area containing the flaw distribution, j is the macroscopic current during, A_o and j_o are normalizing parameters, and j_u and n are again materials parameters. It will be assumed here that the current density below which $P_s \equiv 1$, j_u, is zero. This assumption has the effect that extrapolation of the data to electrode areas many times larger than the test areas leads to specimen survival probabilities going to zero at finite current densities. Since large tubes are known to survive finite current densities, the assumption that $j_u = 0$ is not justified. From the tests reported here j_u could not be determined. The data therefore should not be used to extrapolate to large electrolyte tubes; they can, however, be used for mutual comparison and for putting an upper bound on j_u.

P_s^i for each test, i, is determined by arranging the values found for the N individual tests in increasing order. The median rank position of the ith datum is then [9]:

$$P_s^i = 1 - [(i - 0.3)/(N + 0.4)] \qquad (3)$$

Two different criteria were used to mark the onset of Mode I degradation: the first definition uses the first significant acoustic emission above background; the second definition uses the start of sustained acoustic activity. The reason for considering two different criteria follows from the general acoustic activity pattern when tests are performed with increasing current densities. The first significant acoustic activity occurs at a current density well below the onset of sustained emission, as is shown in Fig. 4. This may be interpreted as follows. An initial flaw population exists in the surface of the elec-

trolyte. Current passage will activate some of these flaws leading to a first flaw extension. The beta aluminas are, however, microstructurally very anisotropic, and it should be expected that local variations in K_{IC}, the critical stress intensity factor, should be encountered by the crack tip. These variations in K_{IC} are especially significant when the flaws are on the order of the grain size, in early flaw growth. Even modest local variations in K_{IC} would strongly affect j_{crit} for that flaw of size , as follows from the recently derived relation [6]:

$$j_{crit} \quad K_{IC}^{4}/\ell \tag{4}$$

One could therefore interpret the acoustic activity patterns such as the one shown in Fig. 4 as due to the establishing of a new flaw population as a result of current passage.

The results of the critical current testing are shown in Fig. 5 and Fig. 6. Figure 5 shows a Weibull plot of the current densities at the first acoustic emission, while Fig. 6 shows a similar plot for the onset of sustained acoustic activity. The differences between the large and the small grain size electrolytes are evident for both data groups. The average critical current densities for the 0.2 cm^2 test specimens were 145 $mAcm^{-2}$ and 640 $mAcm^{-2}$ for the large and the small grain size electrolytes respectively at the first sustained acoustic activity. The differences for the onset of first acoustic actvity are not as large. The data clearly show that Mode I breakdown is initiated at lower average current densities for larger grain size electrolyte. It is interesting to note that the ratio of the average

critical current densities is comparable to that of the average grain size or average largest grain dimension. This would actually be expected on the basis of Eq. 4. The lowest initial current density observed in the set of experiments on the fine grain size material, taking the onset of sustained acoustic activity as the significant initiation of Mode I failure, is 225 mA/cm^2. This puts an upper bound on j_u (Eq. 2) of about 200 mA/cm^2.

4.3 Microstructural examination

The sodium entrance and exit surfaces of polished, large grained electrolytes were examined after electrolysis. Figure 7A shows a silver stained sodium exit surface after a unidirectional charge transfer of 22 A hr/cm^2, at 350°C, with a current density increasing uniform in time from 0 to 7.5 A cm^{-2}. The micrograph reveals preferential degradation along the grain boundaries of large grains. Figure 7B is a stained cross-section of this sample showing how such Mode I degradation extends into the interior of the electrolyte. The silver decoration of similarly used sodium entrance surfaces did not show this type of grain boundary degradation. These observations are in agreement with the acoustic emission data showing lower critical current densities for large grained electrolytes.

The involvement of large grains in failure initation is in general agreement with the trend of mechanical strength reported by Virkar and Gordon [10] on β" aluminas of similar composition but with differing microstructures. In their observation the fracture strength of the solid electrolytes decreases significantly when a substantial fraction of large grains (>120μm) is present.

Further support for the conclusion that large grains have a significant role as preferred sizes or paths for Mode I breakdown was found in electrolytes used in the long-term Na/S cell test of British Rail. Figure 8 shows an optical micrograph of a polished and stained cross-section under reflected light, Fig. 8A, to reveal the microstructure, and with crossed polarizers to reveal the decoration of a Mode I type degradation, Fig 8B. This degradation appears to have followed a string of large grains emerging at the Na electrode interface. It is not possible to specify when this Mode I degradation occurred.

Frequently, Mode I cracks that have not reached the sulfur electrode interface are found in used electrolytes. This strongly suggest that slow subcritical sodium dendrite growth occurs during Na/S cell cycling. It is interesting to note here that in purely mechanical testing Shetty et al. [3] did not find evidence for a stress-corrosion effect, strongly suggesting that mechanical and electromechanical degradation cannot be considered equivalent.

5. Discussion

Although the observations indicate that mechanical and electromechanical failure are not equivalent, it is nevertheless useful to discuss briefly the significance of Eqs. 2 and 4 in the context of the present findings. The particular dependence of j_{crit} on K_{IC}, Eq. 4, permits a comparison of the mechanical reliability, expressed by m in Eq. 1, and electrical reliability expressed by n in Eq. 2. It follows from Eqs. 1, 2 and 4 that $m \simeq 4\ n$. If, for example, one would operate a tube at a current density j_{op}, which is a factor B below

the 50% failure probability current, j_{50}, then one could specify n, and hence m, for a particular level of required survival P_R. Then,

$$n = \left(\ln \ln \frac{1}{P_R} - \ln \ln \frac{1}{0.5} \right) / \ln B \ . \tag{5}$$

Table I lists some examples for m and n, calculated with Eq. 5, when B is 10, 5 or 2, and P_R is 0.95 or 0.99. It is evident from this table that the requirements on reproducibility of mechanical properties of large electrolyte tubes would become very stringent if $B = j_{50}/j_{op}$ becomes less than 5, and an initial crack initiation level of less than 5% cannot be tolerated. Alternatively one might eliminate the weaker electrolyte tubes by subjecting them to a uniform proof stress, σ_p, that is related to the average fracture strength, $\bar{\sigma}$, by

$$\left(\frac{\bar{\sigma}}{\sigma_p} \right)^{4n} = - \ln P_R / \ln 2 \tag{6}$$

The considerations are analogous to those of mechanical proof testing [11] as follows from combining Eqs. 4 and 5. Proof stress testing of electrolytes has also been proposed by Virkar [12]. The present discussion clearly points out what is required of the electrolyte tubes if mechanical and electrical failure were identical. In the case where n, B and P_R are fixed by materials and economic operating conditions then a mechanical or electrical proof testing would be a necessity when

$$|\ln B| < \left| \left(\ln \ln \frac{1}{P_R} \ \ln \ln \frac{1}{0.5} \right) / n \right| . \tag{7}$$

Equation 7 is represented graphically in Fig. 9 for survival probabilities of 0.90, 0.95 and 0.99. Each line of constant P_R separates domain of n and B values in which proof testing is or is not necessary. Since actual ceramics have m (Eq. 1) range between 5 and 20, with m 10 a common value for reasonably well prepared ceramics, one should expect n to be in the neighborhood of 2 or 3, as appears to be the case in the present tests. For a 99% absence of crack initiation events Fig. 9 then indicates that B should be between 5 and 10. Since the Na/S batteries are usually operated around 80 to 100 $mAcm^{-2}$, this would have to put the average Mode I failure initiation around 1 A cm^{-2}. The present experiments, performed on small electrode areas, show an average Mode I initiation threshold of only about 500-600 mA cm^{-2}. Requirements of a low incidence of crack initiation event probability would therefore appear to require either electrical or mechanical proof testing. The most reliable method for proof testing would in fact be one in which the Weibull parameters n and m, and the average failure current density, j_{av}, and average fracture stress, σ_{av}, are determined on electrolyte specimens that are identical to those used in the batteries. The mechanical testing would be one in which the entire tube is stressed uniformally to fracture, so that extrapolation of data is minimal.

A first point that must be emphasized is that the above considerations are only valid under the conditions of strict equivalence of mechanical and electrolytic failure. While all our observations seem to indicate that such equivalence does not fully prevail, it should

that the mechanical properties strongly affect the electrical ones. Since the exact correspondence has not yet been established we should take the above considerations only as a possible worst case, underscoring the necessity for collecting statistical data on full or nearly full scale cells.

A second point that needs some discussion is the definition of electrolyte failure. While electrolytes used in Na/S cells nearly always show some Mode I cracks, even after relatively short use (~ 20A hr/cm^2), often they still can function with virtually no detectable deterioration in cell performance. Thus, the critical current density thresholds reported here use a different failure initiation definition than a battery developer would. Typically, a technological definition uses the appearance of a specified level of non-Faradaic behaviour as a failure criterion. Non-Faradaic currents in Mode I failure are the result of electronic shorting through the sodium filled crack. In laboratory Na/Na cell tests this is manifested by an abrupt voltage drop at constant cell current. These abrupt voltage drops were also observed in the present experiments but they occurred at current densities of around 1 to 1.5 A cm^{-2}. The electronic shorting was in most cases only partial, and the apparent cell resistance change in many cases would be no more than 10%. The correlation between Mode I initiation in laboratory test such as reported here and technologically meaningful electrolyte failure in a Na/S cell is therefore not yet established. However, the present

experiments can be considered suitable for comparison of the effects of microstructure, and for the evaluation of the adequacy of models proposed for the initiation current density thresholds of Mode I degradation.

6. Acknowledgments

This work was supported by the Assistant Secretary for Conservation and Renewables, Office of Advanced Conservation Technology, Electrochemical Systems Research Division of the U. S. Department of Energy under Contract No. W-7405-ENG-48.

Major funding for this work was provided by the Electric Power Research Institute.

Dr. L. Feldman is thanked for the verification of the acoustic emission detection method.

Dr. Sudworth of British Rails is thanked for providing the electrolytes used in actual sodium/sulfur cells.

7. References

1. L. C. De Jonghe, L. Feldman, and A. Buechele, J. Mat. Sci. 16 (1981) 780.
2. R. D. Armstrong, T. Dickinson, and I. Turner, Electrochim. Acta 19 (1974) 187.
3. D. H. Shetty, A. V. Virkar, R. S. Gordon in "Fracture Mechanics of Ceramics," Vol. 4, Proceedings of an International Symposium on Fracture Mechanics of Ceramics, ed. R. C. Bradt, et al., 1978, pp. 651-665.
4. R. H. Richmann and G. J. Tennenhouse, J. Amer. Ceram. Soc., 58 (1975) 63.
5. A. Virkar and L. Viswanatan, J. Amer. Ceram. Soc. 62 (1979) 528.
6. L. Feldman and L. C. De Jonghe, J. Mat. Sci., to be published.
7. C. A. Worrell and B. A. W. Redfern, J. Mat. Sci. 13 (1978) 1515.
8. L. C. De Jonghe and L. Feldman, Mat. Res. Bull. 15 (1980) 777.
9. R. N. Davidge, in "Mechanical Behaviour of Ceramics", Cambridge Univ. Press, 1979.
10. A. Virkar and R. S. Gordon, J. Amer. Ceram. Soc. 58 (1975) 63.
11. A. G. Evans and J. M. Wiederhorn, Int. J. Fracture 10 (1974) 379.
12. A. Virkar and G. Miller, in "Fast Ion Transport in Solids", P. Vashishta, J. N. Mundy, G. K. Shenoy, Eds., Elsevier North-Holland, 1979, pg. 87-90.

Table I. Microstructural Comparison

	Material	
	"10"	"300"
Average grain size	1.1 μm	5.2 μm
Volume fraction grains larger than 10 μm	<0.01	0.83
Average small grain size	0.94 μm	1.1 μm
Average largest dimension of grains > 10 μm	14 μm	54 μm

Table II.

B	$P_R = .95$		$P_R = .99$	
	n	m	n	m
10	1.1	4.4	1.8	7.2
5	1.6	6.4	2.6	10.4
2	3.75	15.	6.1	24

Fig. 1. Comparison of the electrolyte microstructures. Scanning electron micrograph of electrolyte etched in H_3PO_4. XBB 815-4088

Fig. 2. Set-up for the acoustic emission detection experiments in Na/Na cells. XBB 813-2152

Fig. 3. Increase in acoustic activity at the freezing point of sodium under constant of 40 $mAcm^{-2}$. XBL 819 2057

Fig. 4. Typical acoustic activity as a function of time at 350°C, with current density increasing at a constant rate. The first significant acoustic events occur at a current density that is significantly lower than that for sustained emission. XBL 819 2058

Fig. 5. Weibull plot of the current densities at which the first, significant acoustic events are observed. XBL 818-1073

Fig. 6. Weibull plot of the current densities at the onset of sustained acoustic emission. XBL 818-1075

Fig. 7A. Silver stained sodium exit surface after a unidirectional charge transfer of 22 hr/cm^2, at 350°C. The current density increased at a constant rate from 0 to 7.5 A cm^2. XBL 815-4089
7B. Stained cross section of sample shown in Fig. 7A, showing Mode I degradiation extending into the interior of the electrolyte. XBL 817-6529

Fig. 8A. Optical micrograph, of electrolyte cross-section (Na electrode side) from Na/S cell after 121 A hr/cm^2 of charge transfer. Reflected light to several microstructure. XBL 814 3576
8B. Same area as in Fig. 8A, crossed polarizers to reveal Mode I degradiation. The degradation has followed a string of large grains in the middle of the micrograph. The arrow points at a common area in Fig. 8A and B.

Fig. 9. Graphic representation of Equation 7 for the different required survival probabilities, P_R, as a function of Weibull exponent, n, and B (defined in text). XBL 818 1078

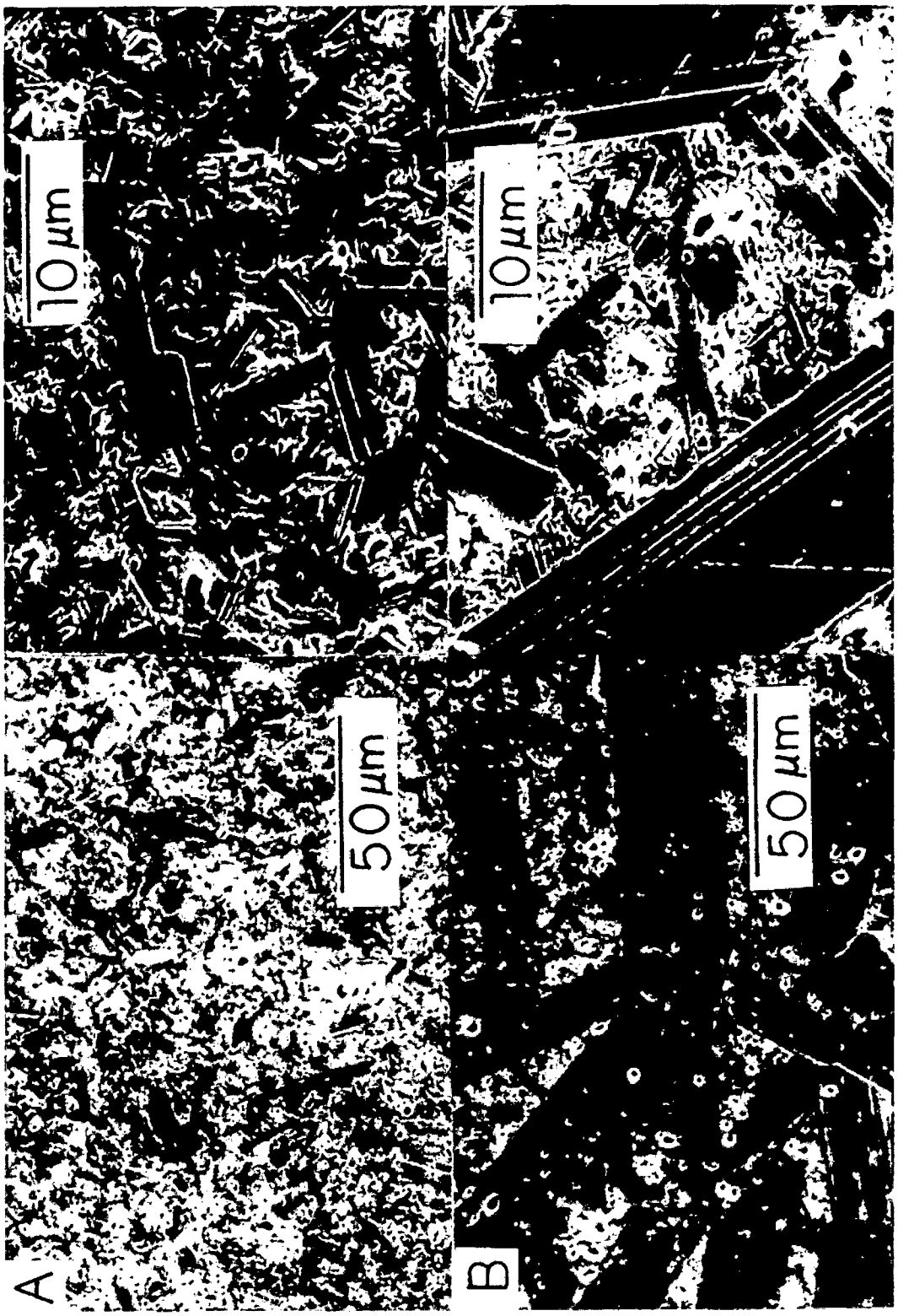

XBB 815-4088

Figure 1

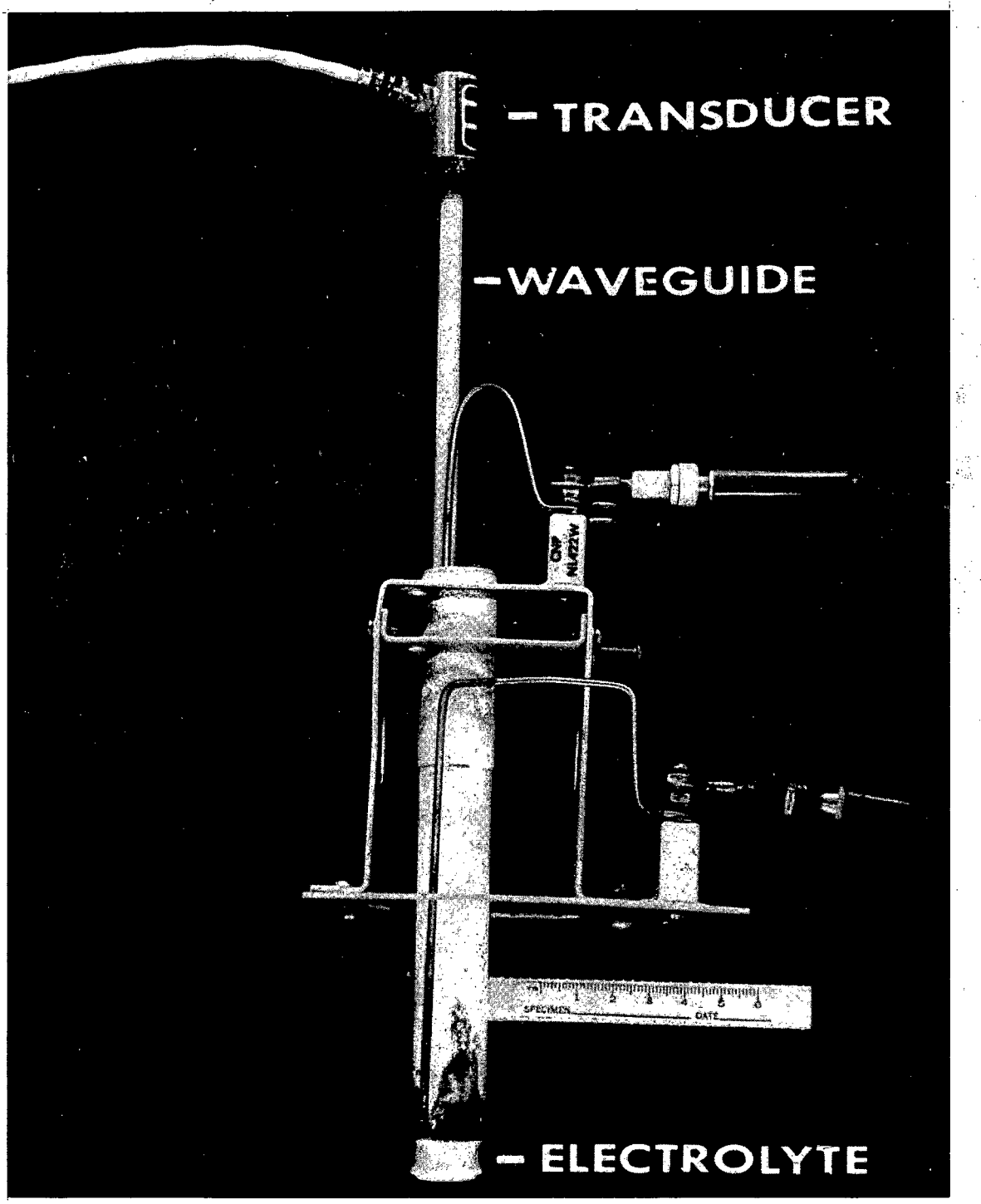

XBB 813-2152

Figure 2

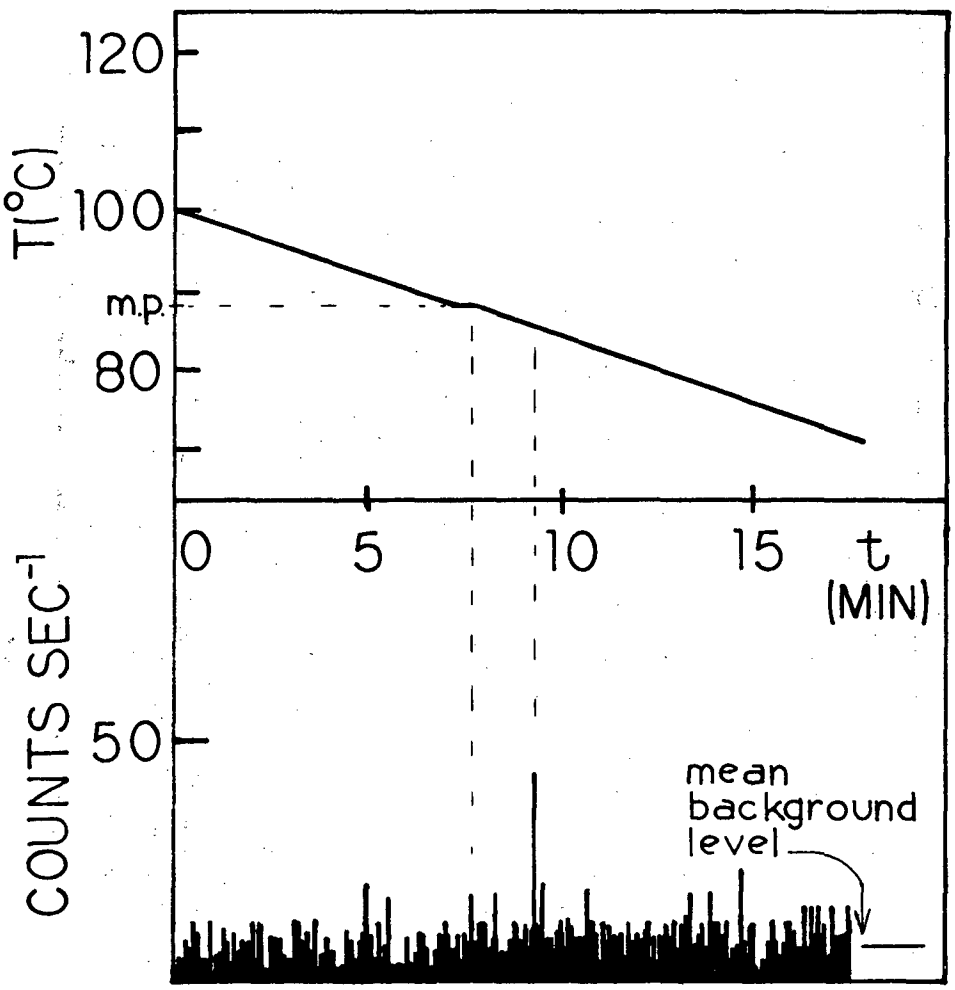

XBL 819-2057

Figure 3

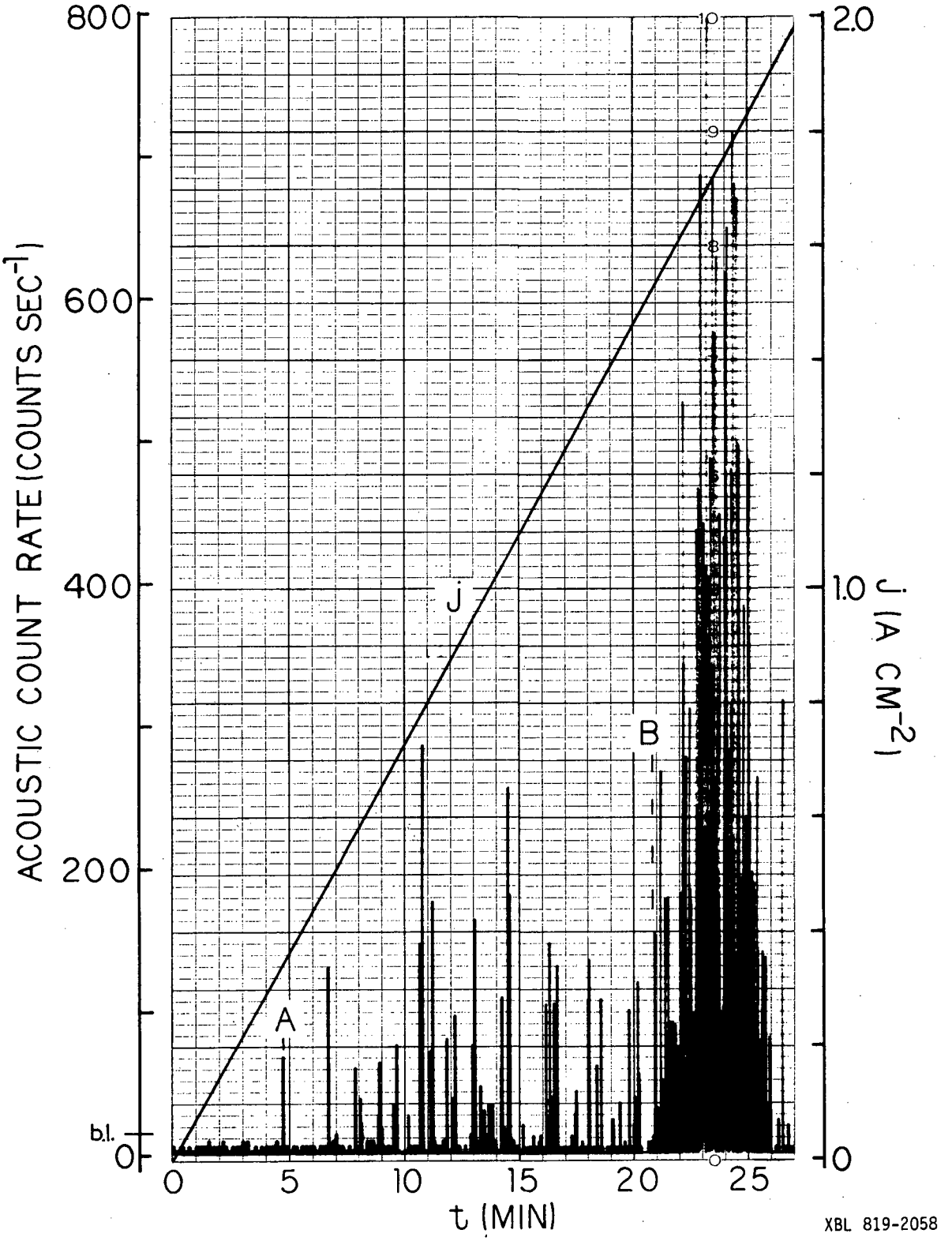
800
600
400
200
b.l.
0
ACOUSTIC COUNT RATE (COUNTS SEC^{-1})
2.0
1.0
0
j (A CM^{-2})
j
A
B
0
5
10
15
20
25
t (MIN)
XBL 819-2058

Figure 4

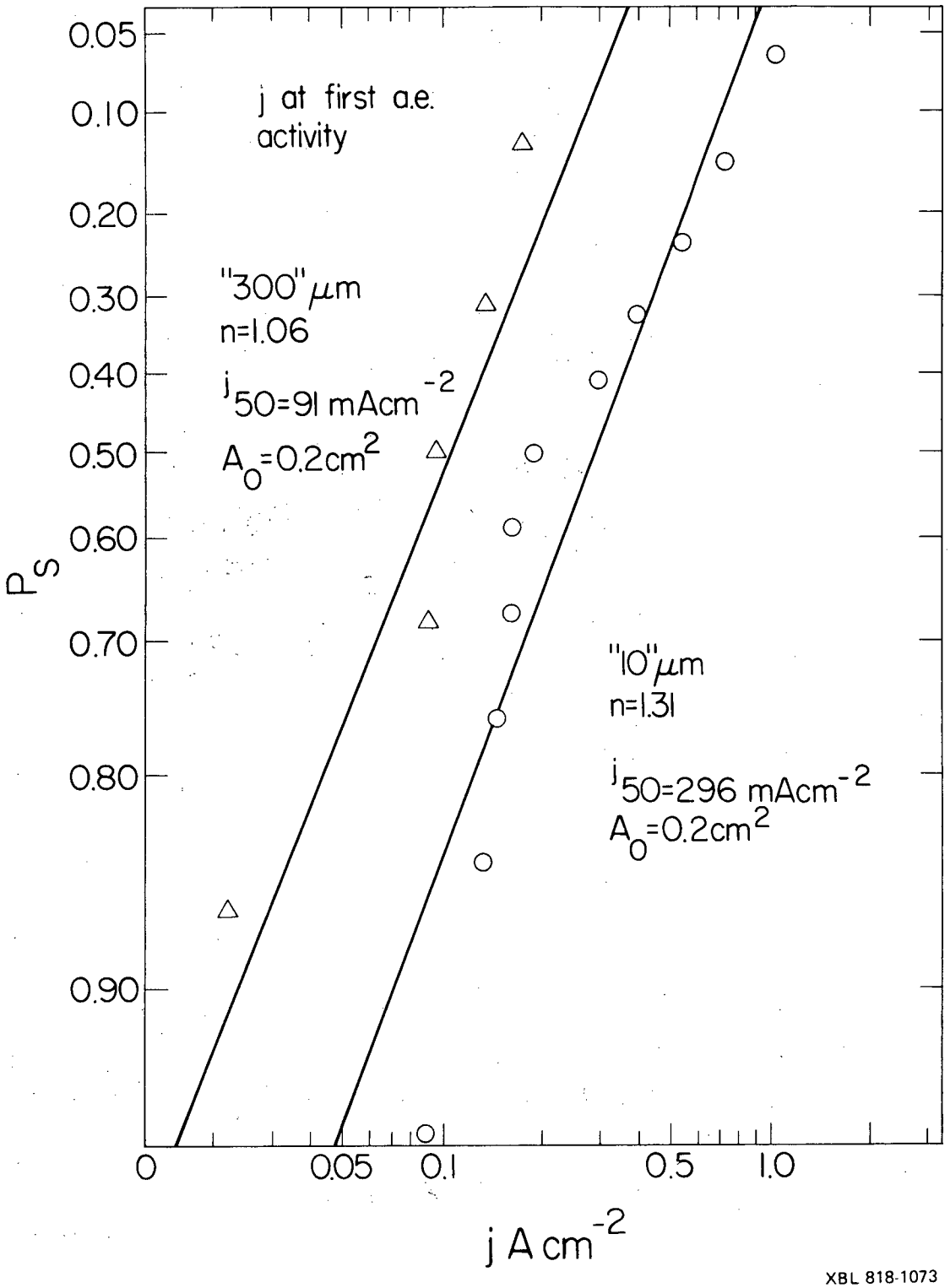
0.05
0.10
0.20
0.30
0.40
0.50
0.60
0.70
0.80
0.90
P_S
j at first a.e. activity
"300" μm
n=1.06
j_{50}=91 mAcm^{-2}
A_0=0.2cm^2
"10" μm
n=1.31
j_{50}=296 mAcm^{-2}
A_0=0.2cm^2
0
0.05
0.1
0.5
1.0
j A cm^{-2}
XBL 818-1073

Figure 5

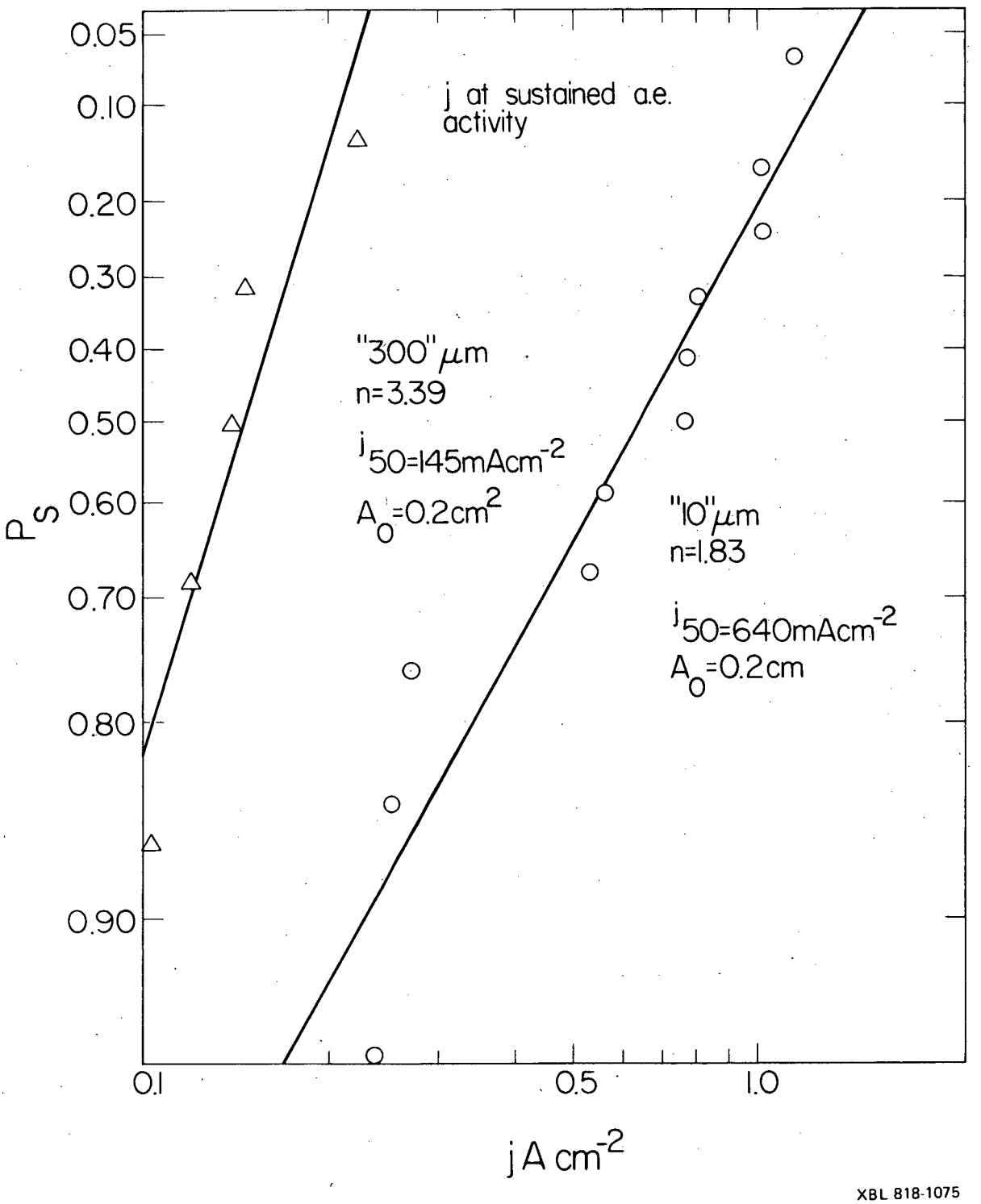
0.05
0.10
0.20
0.30
0.40
0.50
0.60
0.70
0.80
0.90
P_S
j at sustained a.e. activity
"300" μm
n=3.39
j50=145mAcm-2
A0=0.2cm2
"10" μm
n=1.83
j50=640mAcm-2
A0=0.2cm
0.1
0.5
1.0
j A cm-2
XBL 818-1075

Figure 6

XBB 815-4089

Figure 7A

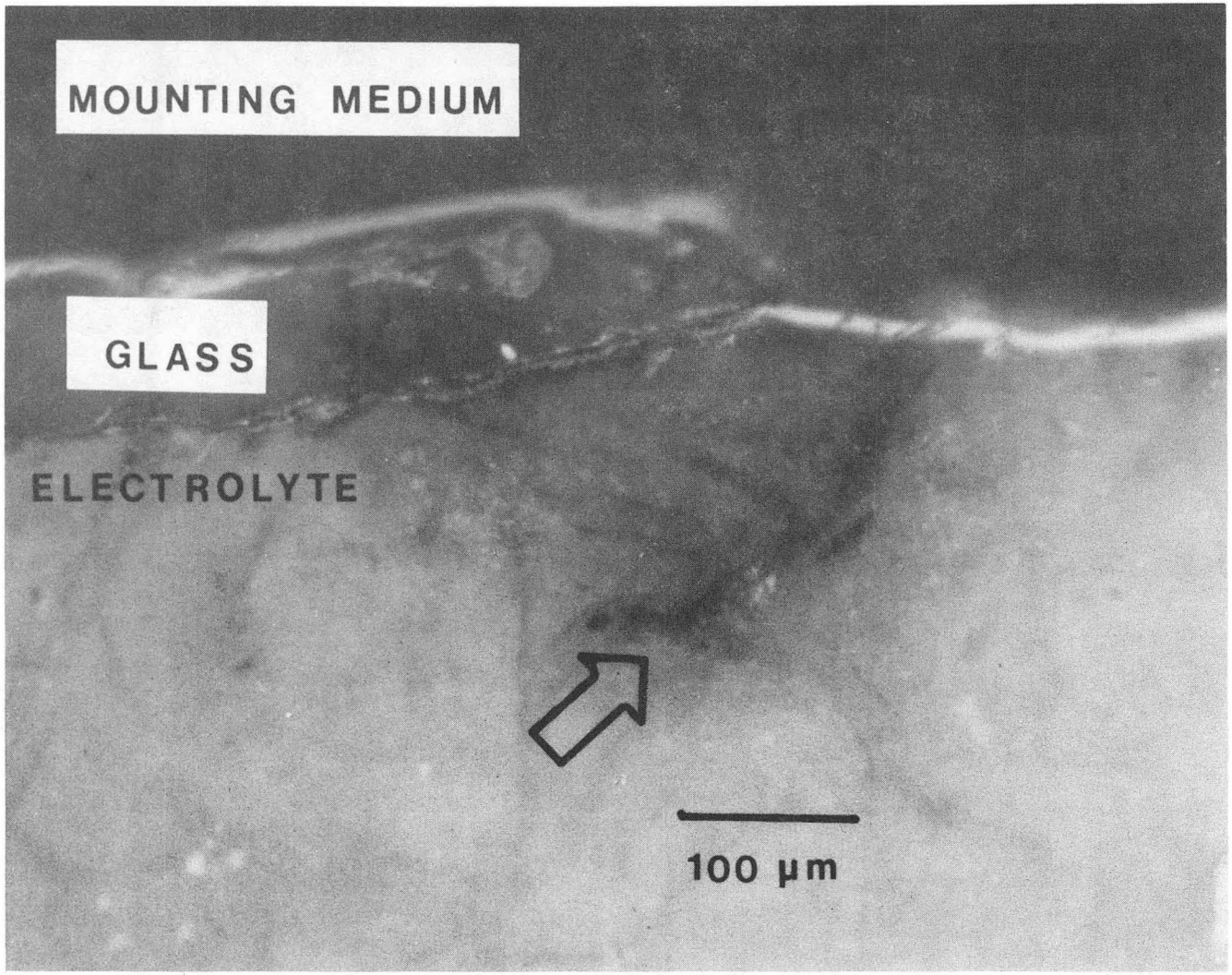

Figure 7B

XBB 817-6529

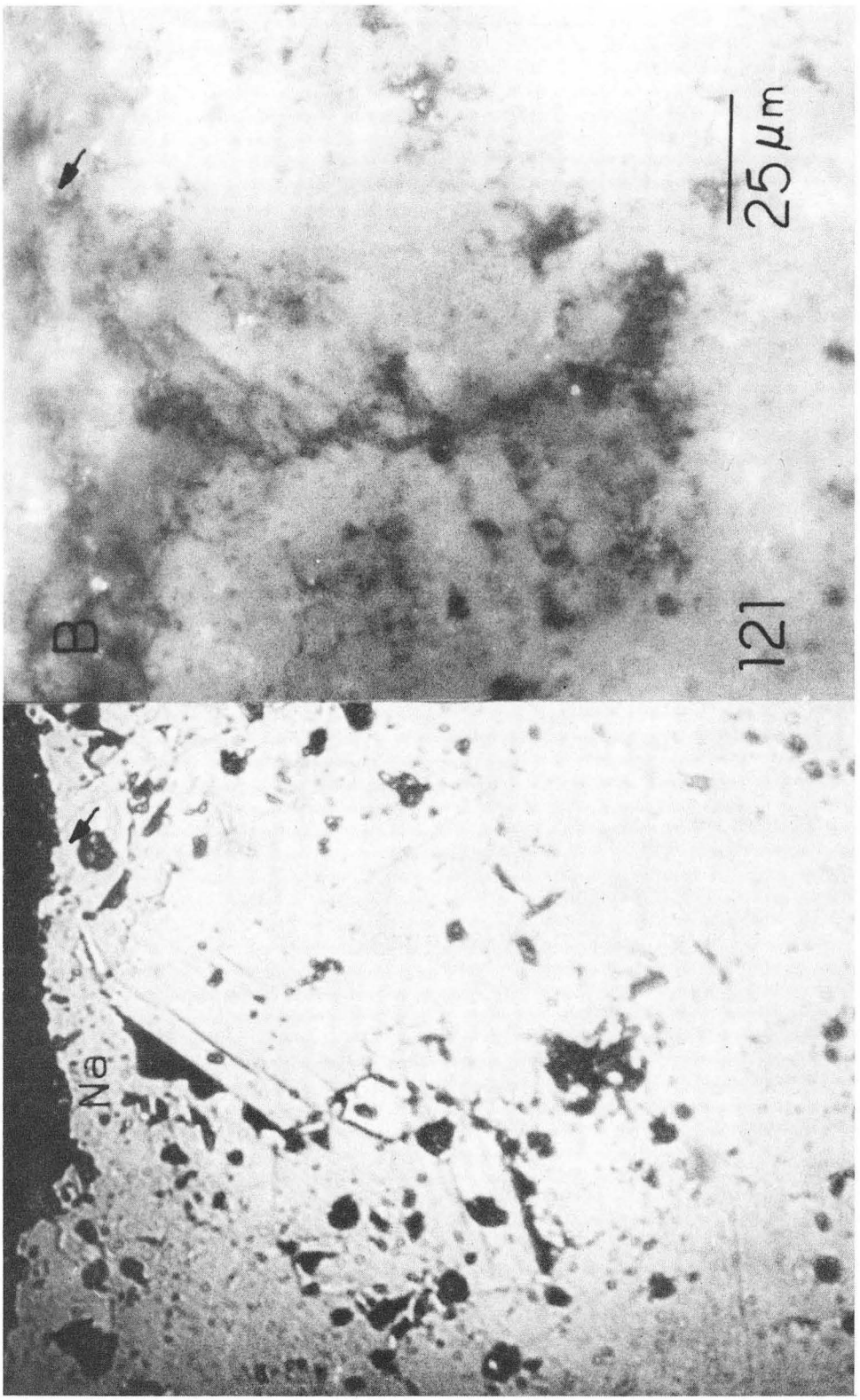

Figure 8A

Figure 8B

XBB 814-3576

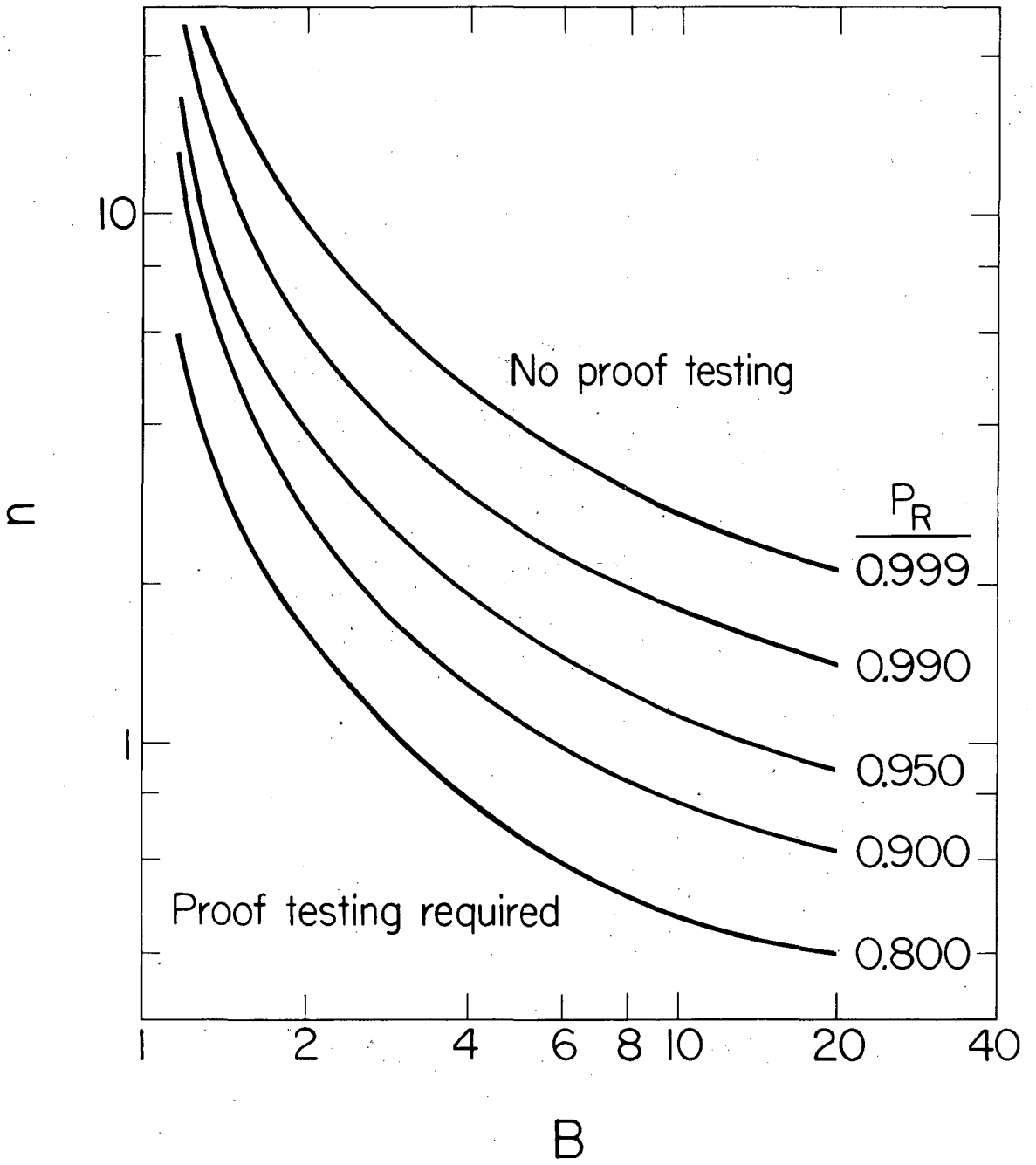

XBL 818-1078

Figure 9

TECHNICAL INFORMATION DEPARTMENT
LAWRENCE BERKELEY LABORATORY
UNIVERSITY OF CALIFORNIA
BERKELEY, CALIFORNIA 94720